Journal of Alloys and Compounds 556 (2013) 153–159

Contents lists available at SciVerse ScienceDirect

Journal of Alloys and Compounds

journal homepage: www.elsevier.com/locate/jalcom

Synthesis of wurtzite ZnS nanoparticles using the microwave assisted solvothermal method

Felipe A. La Porta [a,b,*], Mateus M. Ferrer [c], Yuri V.B. de Santana [c], Cristiane W. Raubach [c], Valéria M. Longo [a], Júlio R. Sambrano [d], Elson Longo [a], Juan Andrés [b], Máximo S. Li [e], José A. Varela [a]

[a] Instituto de Química, UNESP, PO Box 355, 14801-970 Araraquara, SP, Brazil
[b] Department of Analytical and Physical Chemistry, Univ. Jaume I, Castelló de la Plana 12071, Spain
[c] Departamento de Química, UFSCar, PO Box 676, 13565-905 São Carlos, SP, Brazil
[d] Laboratório de Simulação Molecular, UNESP, PO Box 473, 17033-360 Bauru, SP, Brazil
[e] Departamento de Física, USP, PO Box 369, 13560-970 São Carlos, São Paulo, Brazil

ARTICLE INFO

Article history:
Received 31 July 2012
Received in revised form 17 December 2012
Accepted 18 December 2012
Available online 27 December 2012

Keywords:
ZnS
Microwave
Optical properties
Nanoparticles

ABSTRACT

In this article, we report the development of an efficient and rapid microwave assisted solvothermal (MAS) method to prepare wurtzite ZnS nanoparticles at 413 K using different precursors. The materials obtained were analyzed by X-ray diffraction (XRD), X-ray photoelectron spectroscopy (XPS), field emission scanning electron microscopy (FE-SEM), transmission electron microscopy (MET) ultraviolet–visible (UV–vis) and photoluminescence (PL) measurements. The structure, surface chemical composition and optical properties were investigated as a function of the precursor. In addition, effects as well as merits of microwave heating on the processing and characteristics of ZnS nanoparticles obtained are reported. The possible formation mechanism and optical properties of these nanoparticles were also reported.

1. Introduction

In recent years, zinc sulfide (ZnS) has received much attention for its potential applications in optoelectronics [1–3]. ZnS can adopt three phases: cubic sphalerite, hexagonal wurtzite or the rarely observed cubic rock salt. ZnS crystallizes in sphalerite under ambient conditions while the wurtzite polymorph is stable above 1293 K. Both hexagonal wurtzite and cubic sphalerite have wide band gaps of 3.77 eV and 3.72 eV, respectively [4] as well as a high index of refraction (2.27 at 1 μm) and a high transmittance in the visible range [5–10].

The size, shape and synthetic environment are crucial factors in determining the chemical and physical properties of ZnS [11,12]. As the current research is directed toward nanoscale phenomena and technology, the synthesis and characterization of ZnS nanostructures is an active field of worldwide research. With a decreasing particle size, the surface-to-volume ratio becomes sufficiently large so that the stability of the cubic sphalerite and hexagonal wurtzite phases is influenced by the surface energy. On a theoretical basis, it has been suggested that the mean surface energy of a three-dimensional nanoparticle is greater for the sphalerite phase than for the wurtzite phase [13–15]. This result is in agreement with the fact that the low-temperature synthesis yields wurtzite-type ZnS nanoparticles [16–21].

Many methods have been developed to produce ZnS nanomaterials [22–27] with a variety of morphologies [28–31,10,32]. In these syntheses, organic surfactants (polyvinylpyrrolidone, cetyltrimethylammonium bromide, etc.) or assisting molecules (ammonia) [33] are used as templates or structure-directing agents which can control both the growth and morphologies of final products [34]. The surface energy and therefore the crystal structure of the range of ZnS nanoparticles strongly depend on synthesis conditions. In addition, most of the organic surfactants and assisting small molecules are costly, and, in most cases, the pure product was obtained only after the complete removal of surfactants which complicates the experimental process. Therefore, it is important to develop new low cost processing material methods, which are environmentally friendly and possess the possibility for the formation of materials on a micro- and nanoscale with well defined morphologies.

Recently, an alternative method such as the microwave assisted solvothermal (MAS) method has emerged in the field of powder preparation with both expected and unexpected merits; e.g., kinetic enhancement, low reaction temperature and time reduction as well as the control of the overall particle size and aggregation process [35]. Because of their advantages, the use of microwave

* Corresponding author at: Instituto de Química, UNESP, PO Box 355, 14801-970 Araraquara, SP, Brazil. Tel.: +55 16 3301 9892; fax: +55 16 3301 9691.
E-mail address: felipe_laporta@yahoo.com.br (F.A. La Porta).

0925-8388/$ - see front matter © 2012 Elsevier B.V. All rights reserved.
http://dx.doi.org/10.1016/j.jallcom.2012.12.081

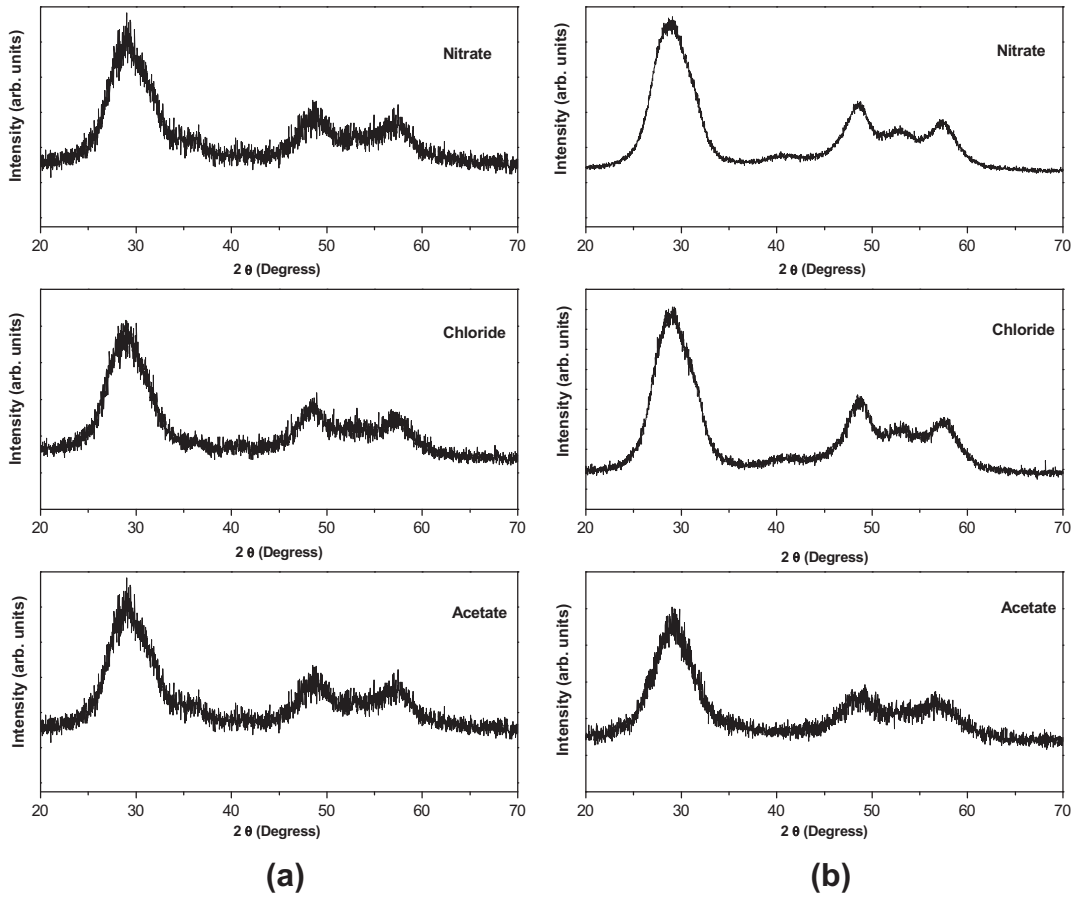

Fig. 1. XRD patterns of ZnS nanoparticles processed at 140 °C using different precursors. A – zinc nitrate; B – zinc chloride and C – zinc acetate.

Table 1
Comparison among synthesis methods.

Method	Temperature (K)	Time (min)	Ref.
Chemical vapor deposition	1373	30	62
Thermolysis	473	30	63
Single-source precursor	543	210–420	64
Evaporation	1573	40	65
Solvothermal	573	720	66
This work	413	1–2	–

radiation during the solvothermal synthesis of inorganic compounds increased rapidly over the past several years [36–39] and several recent comprehensive reviews on microwave-assisted syntheses of nanocrystals have been published [40–44].

Some research groups reported the synthesis of ZnS nanoparticles using the MAS method [19,45–47,12]. In particular, Yao et al. [45] have synthesized ZnS nanospheres by microwave irradiation and have verified that this technique stimulates nanoparticles to spontaneously assemble into a hierarchical structure without template agents. The synthesis of wurtzite ZnS nanorods by the microwave assisted chemical route has been reported by Navaneethan et al. [46]. Shahid et al. [47] reported the microwave assited low temperature synthesis of wurtzite ZnS quantum dots while Savaranan et al. [12] studied the synthesis of cubic ZnS quantum dots, capping and optical–electrical characteristics. Very recently, our group conducted experimental and theoretical studies on the enhanced PL activity of ZnS nanostructures [48,49].

The focus of this research is to study the synthesis of ZnS nanoparticles using the MAS method and to outline the effect of the precursor on the structure, surface chemical composition and optical properties of ZnS nanoparticles; XRD, XPS, UV–vis and PL measurements were employed. The possible formation mechanism and optical properties of these nanoparticles were also reported.

2. Experimental details

2.1. Synthesis

ZnS nanoparticles were synthesized by the efficient MAS method using three precursors (chloride, nitrate and acetate) in ethylene glycol (EG) at 413 K at different times. The typical procedure is described as follows: 7.34 mmol of precursors (zinc nitrate, zinc acetate and zinc chloride) and 15.44 mmol of tetrabutylammonium hydroxide were dissolved in 25 mL of EG and heated to 353 K (solution 1); 7.34 mmol of thiourea were separately dissolved in another 25 mL of EG (solution 2). Under vigorous magnetic stirring, solution 1 was then quickly injected into solution 2. In the sequence, the solution was transferred into a Teflon autoclave which was sealed and placed inside a domestic microwave-solvothermal system (2.45 GHz, maximum power of 800 W). The pH of the reaction for the synthesis of all prepared materials was 10. MAS processing was performed at 140 °C for short times (1 and 2 min). To remove byproducts possibly remaining in the final product, the resulting solution was washed with deionized water and ethanol several times to neutralize the solution pH (≈7), and the precipitates were finally collected followed by thermal treatment at 343 K (24 h).

2.2. Characterizations

The nanoparticles obtained were structurally characterized by XRD using a Rigaku-DMax/2500PC with Cu Kα radiation (λ = 1.5406 Å) in the 2θ range from 10° to 75° at 0.02°/min. XPS was employed to determine the metal content and to analyze its structural conformation using a commercial spectrometer (UNI-SPECS-UHV). Spectra binding energies were corrected using the hydrocarbon component of adventitious carbon fixed at 285.0 eV. The composition of the surface region was determined from the ratio of relative peak areas corrected by sensitivity factors (Scofield) of corresponding elements. Spectra were fitted without placing constraints using multiple Voigt profiles. The morphologies of ZnS nanoparticles were

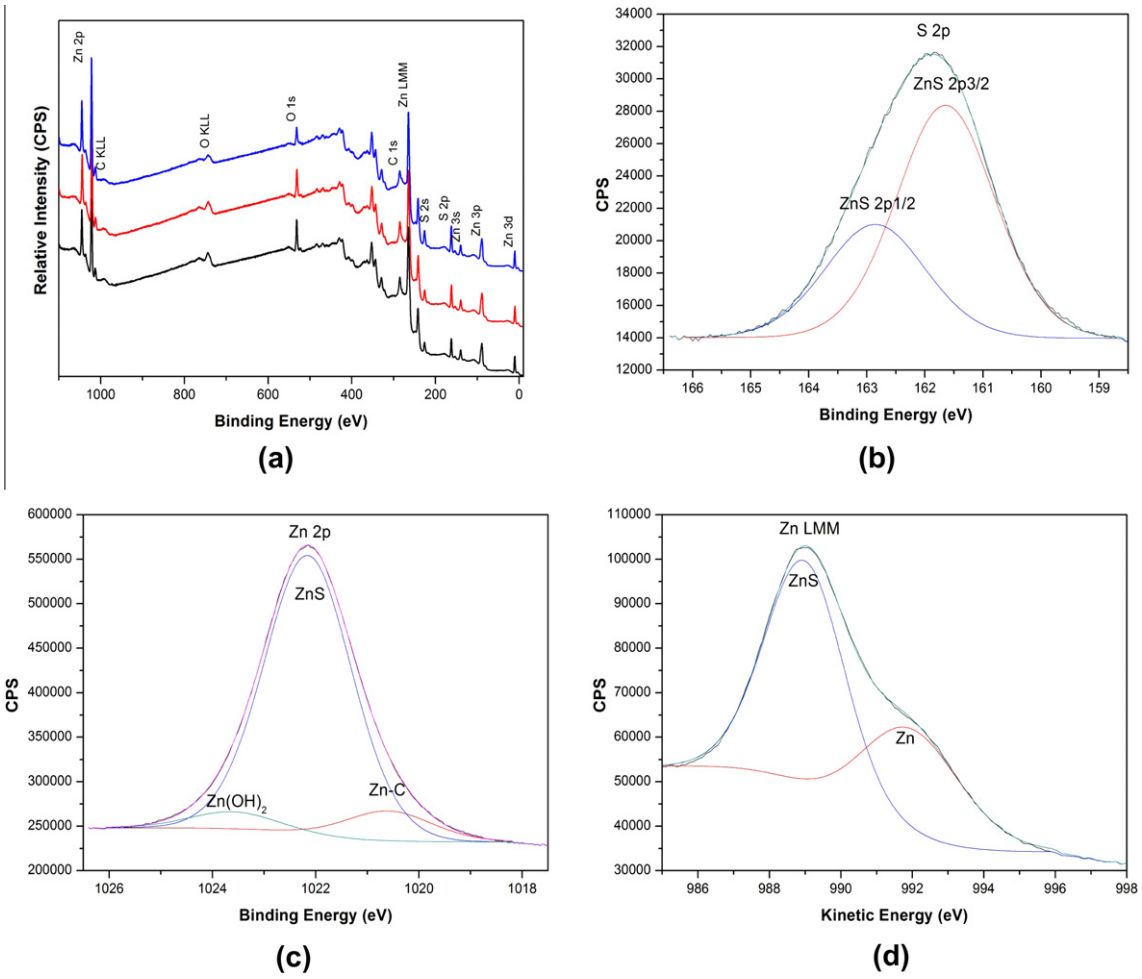

Fig. 2. Typical XPS spectra of synthesized ZnS wurtzite: (a) survey spectrum, (b) S 2p region spectrum, (c) Zn 2p3 region spectrum and (d) Zn LMM region spectrum.

observed by FE-SEM using FEG-VP JEOL. In the sample preparation for the TEM technique, the obtained powders were first dispersed in ethanol using an ultrasonic bath for 20 min. Afterwards, the suspensions were deposited on the copper grids via fast immersion.

Optical properties were analyzed by UV–vis absorption spectra and PL measurements. UV–vis spectra were taken using a Cary 5G spectrophotometer (Varian, USA) in a diffuse reflectance mode. The optical band gap energy (E_{gap}) was calculated by the Kubelka and Munk method and is related to the absorbance and photon energy by the following equation:

$$\alpha h\nu = C_1(h\nu - E_{gap})^n, \quad (1)$$

where α is the linear absorption coefficient of the material, $h\nu$ is the photon energy, C_1 is a proportionality constant, E_{gap} is the optical band gap and n is a constant associated with different kinds of electronic transitions (n = 1/2, 2, 3/2 or 3 for direct allowed, indirect allowed, direct forbidden and indirect forbidden transitions, respectively) [49]. This methodology is based on the transformation of diffuse reflectance measurements to estimate E_{gap} values with good accuracy [50–53]. PL spectra were collected with a Thermal Jarrel-Ash Monospec monochromator and a Hamamatsu R446 Photomultiplier. The 350.7 nm (2.57 eV) exciting wavelength of a krypton ion laser (Coherent Innova) was used with the output of the laser maintained at 200 mW. All measurements were performed at room temperature.

3. Results and discussion

An analysis of XRD patterns depicted in Fig. 1 confirms that all ZnS nanoparticle diffraction peaks can be indexed to the hexagonal structure which is in agreement with the respective Joint Committee on Powder Diffraction Standards (JCPDS) card 36–1450 [52]. Thus, these results indicate that ZnS nanoparticles are crystalline, pure and ordered at long range. The diffraction peaks are significantly broadened because of the very small crystallite size. These results are in very good agreement with other experimental studies [21,48,49]. However, the existence of a cubic ZnS phase solely from XRD patterns cannot be excluded because of the large similarity between cubic and hexagonal ZnS structures.

Microwaves are electromagnetic waves with wavelengths that range between a meter and a millimeter and are selectively absorbed by polar molecules. Although the understanding of the interaction between these waves and matter is limited, it has been hypothesized that an energy transfer process occurs *via* either resonance or relaxation processes; both processes result in rapid heating [53–55].

This procedure is based on dipolar and electrical conduction mechanisms. For the dipolar mechanism, the polar molecules follow the field in the same alignment when a very high frequency electrical field is applied, and then the molecules release enough heat to drive the reaction forward. In the electrical conduction mechanism, the irradiated sample is an electrical conductor and the charge carriers, ions and electrons move through the material under the influence of the electrical field which facilitates polarization within the sample. These induced currents and any electrical resistance will heat the sample [56–58]. This effect provides an advantage for MA techniques which produce faster reaction rates and shorter reaction times and thereby results in an overall reduction in energy consumption [59,60]. Table 1 shows a comparison of ZnS wurtzite phase synthesis data obtained in this work with synthesis data reported in the literature by different methods [61–65].

The samples were characterized using XPS techniques, and spectra are reported in Fig. 2, including (a) the survey spectrum,

Table 2
Quantification of peaks with a ratio of Zn to S for typical XPS spectra of the BEs for ZnS (wurtzite-type) powders at 140 °C using different precursors at around 162 eV for S 2p and 1022 eV for Zn 2p3.

Precursor	BEs	Pos.	FWHM	Area	At%
Survey spectrum					
Nitrate	C 1*s*	285.10	4.651	85942.6	42.88
	O 1*s*	531.35	3.377	65166.8	11.41
	S 2*s*	161.60	3.076	83340.9	23.90
	Zn3*p*	88.85	5.293	112777.5	21.81
Chloride	C 1*s*	285.00	4.179	89854.9	43.03
	O 1*s*	531.25	3.236	98303.4	16.52
	S 2*s*	161.75	3.039	71853.7	19.77
	Zn3*p*	89.00	5.203	11480.1	20.69
Acetate	C 1*s*	285.15	4.288	78861.5	40.93
	O 1*s*	531.65	3.144	113171.7	20.61
	S 2*s*	161.90	2.981	56489.3	16.85
	Zn3*p*	88.65	5.200	107450.0	21.61
S 2p region spectrum					
Nitrate	ZnS $2p_{3/2}$	161.64	1.994	66.66	–
	ZnS $2p_{1/2}$	162.86	2.048	33.34	–
Chloride	ZnS $2p_{3/2}$	161.54	1.925	66.66	–
	ZnS $2p_{1/2}$	162.73	1.954	33.34	–
Acetate	ZnS $2p_{3/2}$	161.89	1.867	66.66	–
	ZnS $2p_{1/2}$	163.05	1.898	33.34	–
Zn 2p3 region spectrum					
Nitrate	Zn–C	120.59	2.000	9.11	–
	ZnS	1022.15	1.998	85.63	–
	$Zn(OH)_2$	1023.61	2.000	5.26	–
Chloride	Zn–C	1020.68	2.000	8.01	–
	ZnS	1022.39	2.000	87.00	–
	$Zn(OH)_2$	1023.93	2.000	4.99	–
Acetate	Zn–C	1020.57	2.000	8.37	–
	ZnS	1022.31	2.000	89.03	–
	$Zn(OH)_2$	1024.23	1.732	2.60	–

(b) S 2p, (c) Zn 2p and (d) Zn LMM. The peaks of Zn and S, together with those of C and O, are clearly visible in survey spectra. From the survey spectrum, we can conclude that the product was highly pure. The binding energies (BE) for wurtzite ZnS powders synthesized by the MAS method at 413 K using different precursors are around 162 eV for S 2p and 1022 eV for Zn 2p3. The kinetic energy for Zn LMM is 989 eV (for more details on the analysis of XPS results, see Fig. 2 and Table 2). These results are consistent with BE values reported by Wagner et al. [65] and Wang et al. [66]. The peak quantification yields a ratio of Zn to S which is in excellent agreement with the stoichiometry of ZnS. These results verify that material surfaces are similar and that the surfactant was removed during the washing process.

FE-SEM and TEM images show that the synthesis route produces ZnS crystalline agglomerate nanoparticles; i.e., ZnS particle facets are quite similar (see Fig. 3). The ZnS nanoparticle morphology suggests that as-formed ZnS clusters are constructed of more primary building particles of different orientations. Fig. 3 confirms that the random aggregation process between small particles results in the formation of irregular-shaped crystallites [49]. For nanocrystals, crystallites agglomerate and form particles with diameters of ~110 nm for a synthesis of 1 min, and there is a greater variation in size with increasing synthesis time. We believe that this aggregation process is related to the increase in effective collision rates between small particles by microwave radiation. However, for an organized solid aggregate, where there is a crystallite-size distribution or particle-density gradient across the solid, the design and architecture become possible upon Ostwald ripening. These mechanisms are responsible for the fast nucleation of ZnS small particles as well as the dissolution of small crystals which

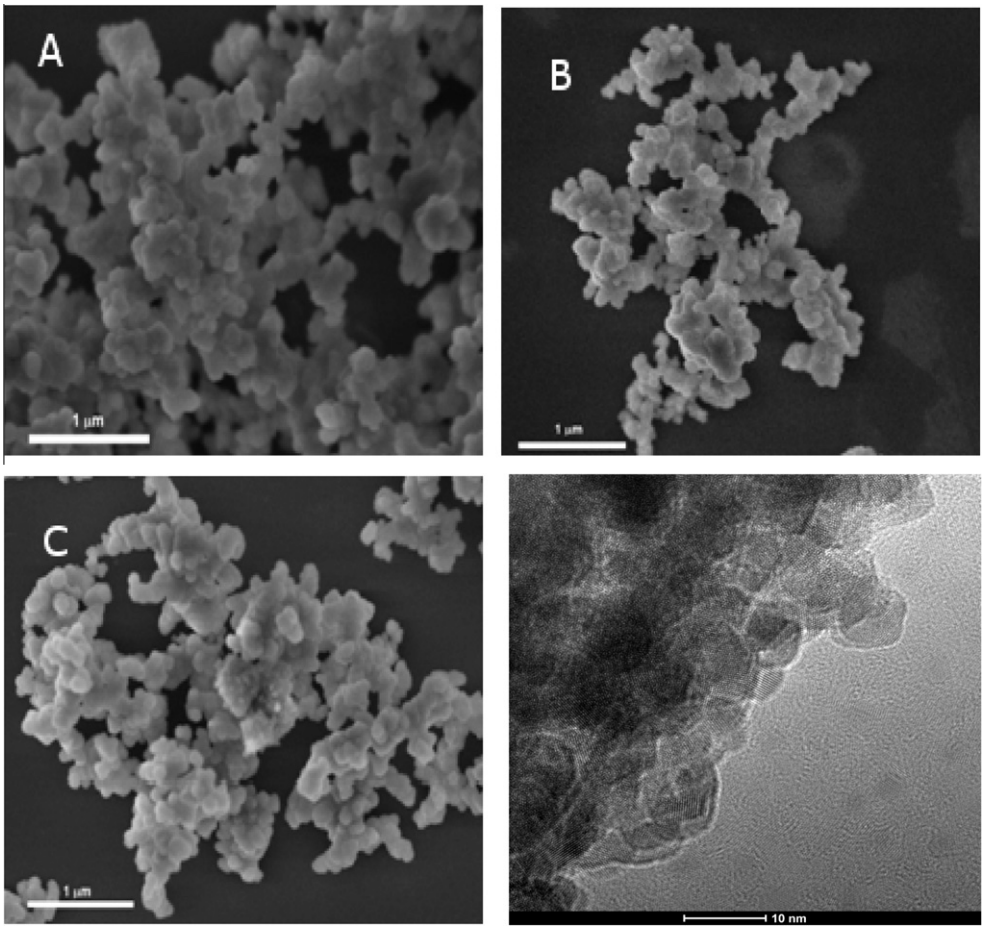

Fig. 3. FEG-SEM image for ZnS samples. (a) A – zinc nitrate; (b) B – zinc chloride and (c) C – zinc acetate.

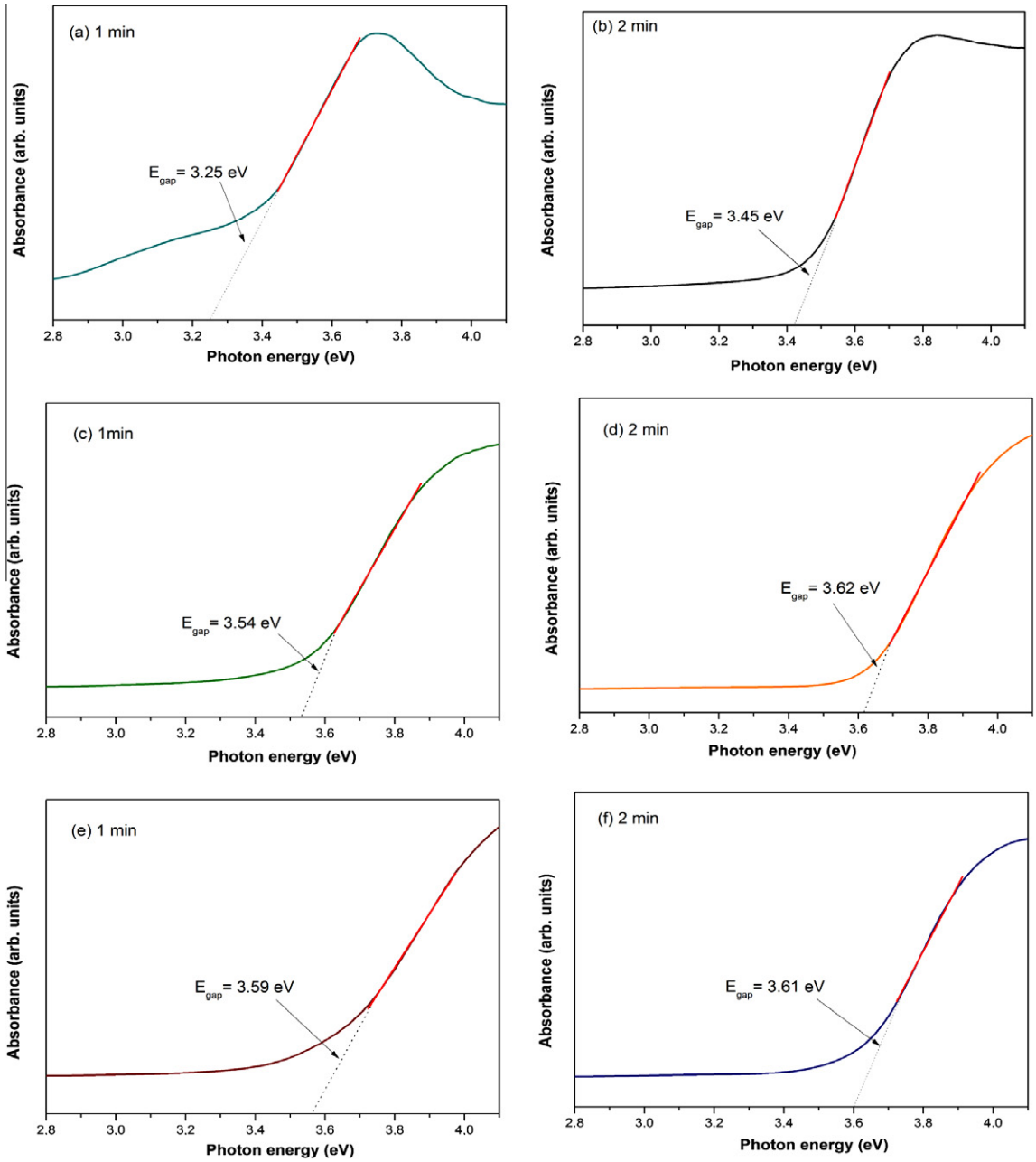

Fig. 4. UV–vis spectra of aggregated crystalline ZnS nanoparticles at 140 °C using different precursors (A – zinc nitrate; B – zinc chloride and C – zinc acetate): (a) A 1 min; (b) A 2 min; (c) B 1 min; (d) B 2 min; (e) C 1 min and (f) C 2 min.

are deposited onto larger crystals. This conclusion is line with previous work of other groups [67,68].

It is a relevant question to ask what types of particles can undergo aggregation. Most growth processes presumably start with the formation of clusters which are colloidally stable as long as no precipitation occurs. Then small nanocrystals are homogeneously nucleated; due to their regular inner structure and the coherent polarization addition as well as a dipole moment, these nanocrystals have a higher Hamaker constant and a coupled lower colloidal stability than their cluster precursors. With decreasing colloidal stabilization (either by concentration, reaction conditions or the consumption of stabilizer), a crystal–crystal addition will occur at first because it is the colloidal species with the highest mutual attraction [69]. After two crystals have been added, anisotropy is generated, and it is a question of interaction energy where the next particle will be added. If the addition is dipole controlled, the next particle will certainly be added along the long axis of the particle [70,71].

A nucleation–dissolution–recrystallization mechanism occurs with the MAS method [72]. which is considered highly sensitive to relative rates of amorphous solid particle dissolution and nucleation of the crystalline phase [73]. As a consequence, this mechanism involves the formation of a high concentration of aggregated nano-particles with predominant growth controlled by the coalescence process. Using density functional calculations, Ghazi et al. [74] determined that growth is an order–disorder–order pattern of a cyclic nature. In this context, the nucleation–dissolution–recrystallization mechanism [72] using the MAS method can be seen as an order–disorder–order process of nature.

Fig. 4a–f shows UV–vis spectra of ZnS powders processed for different time. UV–vis absorption measurements illustrate a variation in the optical band gap values from 3.25 to 3.62 eV for ZnS

nanoparticles. After the electronic absorption process, electrons located in the maximum-energy states in the valence band revert to minimum-energy states in the conduction band under the same point in the Brillouin zone [48,49]. The exponential optical absorption edge and the optical band gap energy are controlled by the degree of structural disorder in the lattice. The decrease in the band gap value can be attributed to defects and local bond distortion as well as intrinsic surface states and interfaces which yield localized electronic levels within the forbidden band gap.

PL emission is considered to be a powerful tool to obtain information on the electronic structure and degree of structural organization of materials at medium range. PL spectra for ZnS samples confirm a broad band covering visible electromagnetic spectra in the range from 400 to 800 nm. Fig. 5 shows PL evolutions of ZnS samples using different zinc salts. The PL behavior of ZnS nanopaticles is dependent upon different precursors and renders a red shift with maximum emission at 478, 505 and 555 nm for syntheses using zinc nitrate, zinc acetate and zinc chloride as precursors, respectively when excited by a 350.7 nm laser line. The use of different wavelengths promotes the excitation of electrons localized at different energy levels within the band gap. With crystallization evolution, the atomic crystalline design renders a better electronic configuration that promotes PL emission. The emission band profile is typical of a multiphonon process; i.e., a system where relaxation occurs by several paths involving the participation of numerous states within the band gap of the material.

First-principles quantum mechanical calculations have shown that the break in lattice symmetry due to structural disorder is responsible for the presence of electronic states in the band gap and reveal that this disordered structure leads to local polarization and a charge gradient in the structure [49]. New levels are formed above the valence band and below the conduction band and are associated with specific ZnS structural disorder. Although these materials are disordered, the details of the band structure in solids are mainly determined by the potential within the unit cell rather than by long range periodicity [75,76].

During the excitation process, the cluster-to-cluster charge-transfer in a crystal containing more than one kind of cluster is characterized by excitations involving electronic transitions from one cluster to another cluster. These studies have shown that ordered–disordered structures in ZnS nanoparticles obtained by using a MAS synthesis have two types of coordination for Zn or S atoms. Sulfur vacancies in a disordered structure with $[ZnS_4]'/[ZnS_3 \cdot V_s^z]$ complex clusters are electron-trapping or hole trapping centers, according to the following equations:

$$[ZnS_4]^x + [ZnS_3 V_s^x] \rightarrow [ZnS_4]' + [ZnS_3 \cdot V_s^{\cdot}] \quad (2)$$

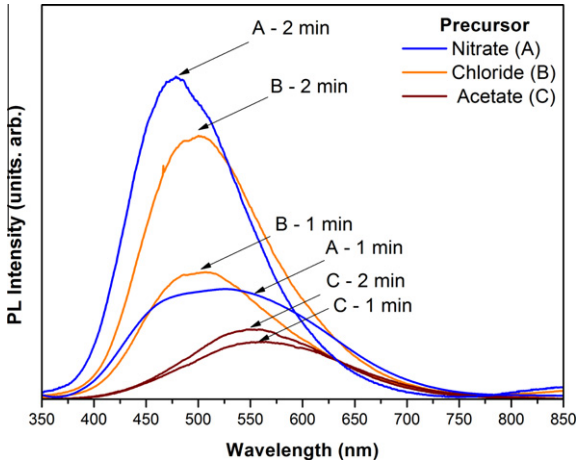

Fig. 5. PL spectra at room temperature of ZnS nanoparticles at 140 °C.

$$[ZnS_4]^x + [ZnS_3 \cdot V_s^{\cdot}] \rightarrow [ZnS_4]' + [ZnS_3 \cdot V_s^{\cdot\cdot}] \quad (3)$$

where a $[ZnS_4]$ donor, $[ZnS_3 \cdot Vs^{\cdot}]$ is a donor/acceptor and $[ZnS_3 \cdot V_s^{\cdot\cdot}]$ is an acceptor. It is assumed that charge redistribution may lead to electron–hole recombination of localized excitons. The structural and electronic reconstructions of all possible combinations of clusters belonging to a specific crystal are essential for the understanding of the CCCT process and its influences on the PL phenomenon [49]. In this case, the increase in the band gap (as shown by UV–vis measurements) promotes the formation of intermediary levels (deep defects) and a shift from blue to red PL emissions as a response to the increase in the crystal size. This series of equations represents complex clusters in structural disordered solids and illustrates the sulfur vacancy occurrences that facilitates the interaction between interclusters. Moreover, this line shape indicates that the confinement effect cannot be considered as the predominant mechanism of luminescence. We can attribute the high PL emission to effects of reduction in the average crystal size, control of the crystal size distribution and possibly to crystallographic orientation promoted by the surfactant.

4. Conclusions

A MAS method to prepare highly crystalline wurtzite ZnS nanoparticles using different precursors is proposed. XRD, XPS, FE-SEM, UV–vis and PL measurements were extensively employed and analyzed to investigate structural and optical properties of the synthesized nanomaterial and to rationalize experimental observations. Our main results are outlined as follows: (i) The PL phenomenon in ZnS at room temperature is directly influenced by structural disorders that yield discrete levels in the forbidden band gap. According to different precursors used, the PL behavior of ZnS causes a red shift which enables the design and control of different colors. The PL emission intensity depends mainly on the interaction of formed structural defects (complex clusters) and the excitation wavelength. These findings confirm that PL is directly associated with localized states in the band gap. (ii) From results reports in this work, we suggest that Ostwald-ripening and self-assemble mechanisms can be responsible for the growth process of these nanocrystals. (iii) This synthesis method has low cost effectiveness and provides high phase purity at a low temperature synthesis in a short time; it is not limited to the system studied and could possibly be followed to prepare other nanostructures. (iv) ZnS nanostructures with a controlled synthesis at a short time have high potential for a low-cost scale-up which facilitates a number of new applications.

Acknowledgments

The authors gratefully acknowledge the support of the Brazilian agencies FAPESP, CNPq and CAPES. J.A. also acknowledges Generalitat Valenciana for Prometeo/2009/053 project, Ministerio de Ciencia e Innovación for project CTQ2009-14541-C02, and Programa de Cooperación Científica con Iberoamerica (Brasil), Ministerio de Educación (PHB2009-0065-PC). We thank Prof. Dr. P. Hammer (LEFE-IQ/UNESP) for their help with the XPS analysis. Special appreciation is extended to Dr. D.P. Volanti for the development of the MAS method.

References

[1] X. Fang, T. Zhai, U.K. Gautam, L. Li, L. Wu, Y. Bando, D. Golberg, Prog. Mater. Sci. 56 (2011) 175–287.
[2] S. Hamad, S.M. Woodley, C.R.A. Catlow, Mol. Simulat. 35 (2009) 1015–1032.
[3] D.V. Talapin, J.-S. Lee, M.V. Kovalenko, E.V. Shevchenko, Chem. Rev. 110 (1) (2010) 389–458.
[4] X.S. Fang, Y. Bando, U.K. Gautam, C.H. Ye, D. Golberg, J. Mater. Chem. 18 (2008) 509–522.

[5] X. Wang, B. Zou, Q. Zhang, A. Lei, W. Zhang, P. Ren, J. Alloys Compd. 509 (2011) 9959–9963.
[6] R. Begum, S. Bhandari, A. Chattopadhyay, Langmuir 28 (25) (2012) 9722–9728.
[7] A.A.A. de Queiroz, M. Martins, D.A.W. Soares, E.J. França, J. Mol. Struct. 873 (2008) 121–129.
[8] B. Sotillo, P. Fernández, J. Piqueras, J. Cryst. Growth 348 (2012) 85–90.
[9] N. Xiao, Q. Dai, Y. Wang, J. Ning, B. Liu, G. Zou, B. Zou, J. Hazard. Mater. 211–212 (15) (2012) 62–67.
[10] X.L. Wang, J.Y. Shi, Z.C. Feng, M.R. Li, C. Li, Phys. Chem. Chem. Phys. 13 (2011) 4715–4723.
[11] N. Jiang, R. Wu, J. Li, Y.F. Sun, J.K. Jian, J. Alloys Compd. 536 (2012) 85–901.
[12] R.S.S. Saravanan, D. Pukazhselvan, C.K. Mahadevan, J. Alloys Compd. 517 (2012) 139–148.
[13] S. Li, G.W. Yang, J. Phys. Chem. C 114 (2010) 15054–15060.
[14] Z. Wang, L.L. Daemen, Y. Zhao, C.S. Zha, R.T. Downs, X. Wang, Z.L. Wang, R.J. Hemley, Nat. Mater. 4 (2005) 922–927.
[15] H. Zhang, F. Huang, B. Gilbert, J.F. Banfield, J. Phys. Chem. B 107 (2003) 13051–13060.
[16] F. Huang, J.F. Banfield, J. Am. Chem. Soc. 127 (2005) 4523–4529.
[17] W. Liu, Mater. Lett. 60 (2006) 551–554.
[18] K. Murakoshi, H. Hosokawa, S. Yanagida, Jpn. J. Appl. Phys. 38 (1999) 522–527.
[19] J.Q. Sun, X.P. Shen, K.M. Chen, Q. Liu, W. Liu, Solid State Commun. 147 (2008) 501–504.
[20] H. Tong, Y.J. Zhu, L.X. Yang, L. Li, L. Zhang, J. Chang, L.Q. An, S.W. Wang, J. Phys. Chem. C 111 (2007) 3893–3900.
[21] Y. Zhao, Y. Zhang, H. Zhu, G.C. Hadjipanayis, J.Q. Xiao, J. Am. Chem. Soc. 126 (2004) 6874–6875.
[22] X. Liang, L. Xing, J. Xiang, F. Zhang, J. Jiao, L. Cui, B. Song, S. Chen, C. Zhao, H. Sai, Cryst. Growth Des. 12 (2012) 1173–1179.
[23] J. Cao, J. Yang, Y. Zhang, Y. Wang, L. Yang, D. Wang, Y. Liu, X. Liu, Z. Xie, Opt. Mater. 32 (2010) 643–647.
[24] N. Goswami, P. Sen, J. Mater. Sci. 47 (2012) 2903–2909.
[25] C. Cheng, G. Xu, H. Zhang, J. Cao, P. Jiao, X. Wang, Mater. Lett. 60 (2006) 3561–3564.
[26] Y.J. Zhang, H.R. Xu, Q.B. Wang, Chem. Commun. 46 (2010) 8941–8943.
[27] S.H. Choi, K. An, E.G. Kim, J.H. Yu, J.H. Kim, T. Hyeon, Adv. Funct. Mater. 19 (2009) 1645–1649.
[28] J. Joo, H.B. Na, T. Yu, J.H. Yu, Y.W. Kim, F.X. Wu, J.Z. Zhang, T. Hyeon, J. Am. Chem. Soc. 125 (2003) 11100–11105.
[29] Z.T. Deng, H. Yan, Y. Liu, Angew. Chem. Int. Ed. 49 (2010) 8695–8698.
[30] X.S. Fang, U.K. Gautam, Y. Bando, B. Dierre, T. Sekiguchi, D. Golberg, J. Phys. Chem. C 112 (2008) 4735–4742.
[31] G. Li, J. Zhai, D. Li, X. Fang, H. Jiang, Q. Donga, E. Wang, J. Mater. Chem. 20 (2010) 9215–9219.
[32] N. Xiao, Q. Dai, Y. Wang, J. Ning, B. Liu, G. Zou, B. Zou, J. Hazard. Mater. 211–212 (2012) 62–67.
[33] X. Fang, Y. Bando, U.K. Gautam, T. Zhai, H. Zeng, X. Xu, M. Liao, D. Golberg, Crit. Rev. Solid State Mater. Sci. 34 (2009) 190–223.
[34] D.E. Clark, D.C. Folz, J.K. West, Mater. Sci. Eng. A 287 (2000) 153–158.
[35] E.T. Thostenson, T.-W. Chou, Composites Part A 30 (1999) 1055–1071.
[36] Z.H. Liang, Y.J. Zhu, Chem. Lett. 33 (2004) 1314–1315.
[37] M.L. Moreira, J. Andres, J.A. Varela, E. Longo, Cryst. Growth Des. 9 (2009) 833–839.
[38] M. Godinho, C. Ribeiro, E. Longo, E.R. Leite, Cryst. Growth Des. 8 (2008) 384–386.
[39] D.P. Volanti, M.O. Orlandi, J. Andres, E. Longo, Cryst. Eng. Commun. 12 (2011) 1696–1699.
[40] M. Baghbanzadeh, L. Carbone, P.D. Cozzoli, C.O. Kappe, Angew. Chem. Int. Ed. 50 (2011) 11312–11359.
[41] I. Bilecka, M. Niederberger, Nanoscale 2 (2010) 1358–1374.
[42] M. Tsuji, M. Hashimoto, Y. Nishizawa, M. Kubokawa, T. Tsuji, Chem. Eur. J. 11 (2005) 440–452.
[43] G.A. Tompsett, W.C. Conner, K.S. Yngvesson, ChemPhysChem 7 (2006) 296–319.
[44] J. Klinowski, F.A.A. Paz, P. Silva, J. Rocha, Dalton Trans. 40 (2011) 321–330.
[45] Q.-Z. Yao, G. Jin, G.-T. Zhou, Mater. Chem. Phys. 109 (2008) 164–168.
[46] M. Navaneethan, J. Archana, K.D. Nisha, S. Ponnusamy, M. Arivanandhan, Y. Hayakawa, C. Muthamizhchelvan, Mater. Lett. 66 (2012) 276–279.
[47] R. Shahid, M.S. Toprak, M. Muhammed, J. Solid State Chem. 187 (2012) 130–133.
[48] Y.V.B. Santana, C.W. Raubach, M.M. Ferrer, F. La Porta, J.R. Sambrano, V.M. Longo, E.R. Leite, E. Longo, J. Appl. Phys. 110 (2011) 123507–123515.
[49] F.A. La Porta, M.M. Ferrer, Y.V.B. Santana, C.W. Raubach, V.M. Longo, J.R. Sambrano, E. Longo, J. Andrés, M.S. Li, J.A. Varela, Current Phys. Chem., in press.
[50] A.E. Morales, E.S. Mora, U. Pal, Rev. Mex. Fis. S 53 (5) (2007) 18–22.
[51] L.S. Cavalcante, V.M. Longo, J.C. Sczancoski, M.A.P. Almeida, A.A. Batista, J.A. Varela, M.O. Orlandi, E. Longo, M.S. Li, Cryst. Eng. Commun. 14 (2012) 853–868.
[52] E.H. Kisi, M.M. Elcombe, Acta Crystallogr. C 45 (1989) 1867–1870.
[53] X.H. Liao, N.Y. Chen, S. Xu, S.B. Yang, J.J. Zhu, J. Cryst. Growth 252 (2003) 593–598.
[54] A. Lagashetty, V. Havanoor, S. Basavaraja, S.D. Balaji, A. Venkataraman, Sci. Technol. Adv. Mater. 8 (2007) 484–493.
[55] R.S. Varma, Green Chem. 1 (1999) 43–55.
[56] E.K. Nyutu, C.H. Chen, S. Sithambaram, V.M.B. Crisostomo, S.L. Suib, J. Phys. Chem. C 112 (2008) 6786–6793.
[57] M.N. Nadagouda, T.F. Speth, R.S. Varma, Acc. Chem. Res. 44 (2011) 469–478.
[58] X.S. Fang, Y. Bando, M. Liao, U.K. Gautam, C. Zhi, B. Dierre, B. Liu, T. Zhai, T. Sekiguchi, Y. Koide, D. Golberg, Adv. Mater. 21 (2009) 2034–2039.
[59] T. Kuzuya, Y. Tai, S. Yamamuro, K. Sumiyama, Sci. Technol. Adv. Mater. 6 (2005) 84–90.
[60] B.Y. Geng, X.W. Liu, J.Z. Ma, Q.B. Du, L.D. Zhang, Appl. Phys. Lett. 90 (2007) 183106.
[61] L. Hou, F.M. Gao, Mater. Lett. 65 (2011) 500–503.
[62] M.B. Mohamed, K.M. AbouZeid, V. Abdelsayed, A.A. Aljarash, M.S. El-Shall, ACS Nano 4 (2010) 2766–2772.
[63] V. Polshettiwar, M.N. Nadagouda, R.S. Varma, Aust. J. Chem. 62 (2009) 16–26.
[64] Q.Y. Lu, F. Gao, S. Komarneni, J. Mater. Res. 19 (2004) 1649–1655.
[65] C.D. Wagner, W.W. Riggs, L.E. Davis, J.F. Moulder, G.E. Muilenberg, Handbook of X-ray Photoeclectron Spectroscopy; Physical Electronics Division, Perkin–Elmer Corporation, Wellesley, MA, 1979.
[66] G.-T. Zhou, X. Wang, J.C. Yu, Cryst. Eng. Commun. 5 (2005) 1761–1765.
[67] M. Muruganandham, R. Amutha, E. Repo, M. Sillanpää, Y. Kusumoto, Md. Abdulla-Al-Mamun, J. Photochem. Photobiol. A 216 (2010) 133–141.
[68] L.H. Oliveira, A.P. Moura, T.M. Mazzo, M.A. Ramirez, L.S. Cavalcante, W. Avansi, V.R. Mastelaro, E. Longo, J.A. Varela, Mater. Chem. Phys. 136 (2012) 130–139.
[69] L. Bergström, Adv. Colloid Interface Sci. 70 (1997) 125–169.
[70] H. Colfen, M. Antonietti, Mesocrystals and Nonclassical Crystallization, John Wiley & Sons Ltd, England, 2008.
[71] V.M. Longo, L.S. Cavalcante, E.C. Paris, J.C. Sczancoski, P.S. Pizani, M.S. Li, J. Andres, E. Longo, J.A. Varela, J. Phys. Chem. C 115 (2011) 5207–5219.
[72] Z.J. Luo, H.M. Li, H.M. Shu, K. Wang, J.X. Xia, Y.S. Yan, Cryst. Growth Des. 8 (2008) 2275–2281.
[73] J.G. Yu, H.T. Guo, S.A. Davis, S. Mann, Adv. Funct. Mater. 16 (2006) 2035–2041.
[74] S.M. Ghazi, S. Zorriasatein, D.G. Kanhere, J. Phys. Chem. A 113 (2009) 2659–2662.
[75] V.M. Longo, L.S. Cavalcante, M.G.S. Costa, M.L. Moreira, A.T. de Figueiredo, J. Andres, J.A. Varela, E. Longo, Theor. Chem. Acc. 124 (2009) 385–394.
[76] M.L. Moreira, E.C. Paris, G.S. Nascimento, V.M. Longo, J.R. Sambrano, V.R. Mastelaro, M.I.B. Bernardi, J. Andrés, J.A. Varela, E. Longo, Acta Mater. 57 (2009) 5174–5185.